In-vivo magnetic recording of neuronal activity

Laure Caruso[1], Thomas Wunderle[2], Christopher Murphy Lewis[2], Joao Valadeiro[3,4], Vincent Trauchessec[1], Josué Trejo Rosillo[1], José Pedro Amaral[3,4], Jianguang Ni[2], Claude Fermon[1], Susana Cardoso[3,4], Paulo Peixeiro Freitas[3,4], Pascal Fries[2,5], Myriam Pannetier-Lecoeur[1]*

[1]SPEC, CEA, CNRS, Université Paris-Saclay, CEA Saclay 91191 Gif-sur-Yvette Cedex, France.

[2]Ernst Strüngmann Institute (ESI) for Neuroscience in Cooperation with Max Planck Society, Deutschordenstraße 46, 60528 Frankfurt, Germany.

[3]Instituto de Engenharia de Sistemas de Computadores-Microsystems and Nanotechnology (INESC-MN), Rua Alves Redol, No. 9, Lisboa 1000-029, Portugal.

[4]Instituto Superior Técnico IST, Physics Department, Universidade de Lisboa, Lisbon 1049-001, Portugal.

[5]Donders Institute for Brain, Cognition and Behaviour, Kapittelweg 29, 6525 EN Nijmegen, Netherlands.

*corresponding authors: myriam.lecoeur@cea.fr, pascal.fries@esi-frankfurt.de

SUMMARY

Neuronal activity generates ionic flows and thereby both magnetic fields and electric potential differences, i.e. voltages. Voltage measurements at (sub)cellular, meso- and macroscopic level constitute electrophysiology. However, each voltage recording suffers from the isolating and smearing properties of the tissue between source and sensor, is blind to ionic flow direction, and reflects the difference between two electrodes, complicating interpretation, specifically of signal correlations. Magnetic field measurements could overcome these limitations, but have been essentially limited to magnetoencephalography (MEG), using centimeter-sized, helium-cooled extracranial sensors. Here, we report on *in-vivo* magnetic recordings of neuronal activity in the visual cortex of cats with *magnetrodes*, specially developed needle-shaped probes carrying micron-sized, non-cooled magnetic sensors based on spin electronics. Event-related magnetic fields inside the neuropil were on the order of several nanoteslas, informing biophysically detailed neural network models, MEG source models and efforts to measure neuronal magnetic fields by other means, e.g. through MRI.

KEYWORDS

Magnetic fields, magnetoencephalography, MEG, spin electronics, magnetic sensors.

HIGHLIGHTS

- Spin-electronics based probes achieve local magnetic recordings inside the neuropil
- Magnetic field recordings were performed *in-vivo,* in anesthetized cat visual cortex
- Event-related fields (ERFs) to visual stimuli were up to several nanoteslas in size
- ERFs could be detected after averaging less than 200 trials

IN BRIEF

Caruso *et al.* report *in-vivo*, intra-cortical recordings of magnetic fields that reflect neuronal activity, using *magnetrodes*, i.e. micron size magnetic sensors based on spin electronics.

INTRODUCTION

Neuronal activity entails ionic flows across the cell membrane and along dendrites. This electrical activity can be measured extra-cellularly or intra-cellularly by microelectrodes (Kandel et al., 2000) which are either thin metallic micro-wires, or glass pipettes containing an ionic solution, to realize a conductive interface between the local brain tissue and the recording instrumentation. Intracellular recordings directly reveal the transmembrane voltage or current of an isolated neuron, but intracellular recordings *in-vivo* are difficult in practice and often only short measurements of single neurons are feasible. Extracellular recordings, on the other hand, measure the aggregate fluctuations in voltage arising from the net neuronal activity around the electrode's tip, with respect to a reference electrode (Buzsaki et al., 2012). Microelectrodes inside the neuropil record action potentials and local field potentials (LFPs), electrocorticographic electrodes provide mesoscopic LFPs, and scalp electrodes deliver the electroencephalographic (EEG) signal. Combining many electrodes into planar (Maynard et al., 1997) or laminar arrays (Lewis et al., 2015) allows for the study of whole brain networks and their dynamics in the intact brain (Buzsaki et al., 2004).

The electric currents flowing through the active neuropil also give rise to a magnetic signature. Magnetoencephalography (MEG) (Cohen, 1968; Cohen, 1972) is a non-invasive method to measure the magnetic fields of active neuronal populations during perceptual or cognitive tasks in the healthy or diseased brain. This technique uses Superconducting Quantum Interference Devices (SQUIDs) cooled down to the temperature of liquid helium (4.2 K). The apparatus

necessary for this cooling imposes a distance to the cortical surface of 3 to 5 cm in *in-vivo* configurations. The spatial resolution is typically better than for EEG recordings, but even under optimal conditions still lies in the order of several mm^3, with signal amplitudes in the femtotesla (10^{-15}T) to picotesla (10^{-12}T) range.

Local magnetic recordings of the neuronal activity could be a complementary technique to electrophysiology, because the magnetic signal provides interesting properties in addition to those realized by the electric signal. Contrary to electric fields, which strongly depend on the dielectric properties of the tissue between neuronal sources and the recording electrode, magnetic fields travel through tissue without distortion, because the respective permeability is essentially the same as free space (Barnes and Greenbaum, 2006). Therefore, magnetic fields are only attenuated by the distance to the current source. Ionic flows and the corresponding magnetic fields are likely largest inside neurons. As those magnetic fields pass through the cell membrane without attenuation, extracellular magnetic field measurements might provide functionally intracellular measurements without impaling the neuron. Moreover, while electrophysiological recordings yield scalar values, local magnetic recordings yield information about both amplitude and direction of current sources. Thereby, they might allow the precise localization of the source of neuronal activity at a given moment in time in the 3D volume of the brain. Furthermore, electrodes always measure the electric potential relative to a reference electrode, and the position and type of reference can substantially influence the measured signal. Moreover, in multi-electrode recordings, all channels typically share the same reference, which poses a problem for analyses of functional connectivity, because the resulting signals are not independent. *Magnetrodes,* presented in this work, provide an elegant solution, because the recorded magnetic

signals are reference-free, and therefore allow for an unbiased measure of connectivity and information flow throughout the brain.

In order to minimize tissue damages, implantable magnetic probes require a needle shape and the miniaturization of the magnetic sensors, while maintaining a very high sensitivity at physiological temperature. Approaches to record the magnetic biological signal closer to the sources than MEG have been successfully realized by using small SQUIDs (Magnelind, 2006), atomic magnetometers (Sander et al., 2012) or winded coils (Roth and Wikswo, 1985) and very recently with nitrogen-vacancy centers in diamond on a living invertebrate (Barry et al., 2016). However, limitations due to the millimeter size of the sensors or to its operating conditions never allowed penetration into the neuropil nor recording at distances of merely tens of microns from the active cells.

RESULTS

Development and fabrication of micron-size magnetic sensors based on spin electronics for *in-vivo* recordings

Spin electronics (Baibich et al., 1988) offers the capability to reduce magnetic sensors to micron size and to reach sensitivity in the sub-nanotesla range while working at body temperature and thereby avoiding bulky vacuum isolation. Spin electronics sensors have been proposed for *in-vitro* measurements of magnetic neuronal signals but have faced direct electrical coupling (Amaral et al., 2011). We have designed Spin Valve (Dieny at al., 1991) Giant Magneto-Resistance (GMR) sensors consisting of 5 segments of 4x30 μm^2 arranged in a meandering configuration on silicon substrate that was ground to a thickness of 200 µm and etched to form a needle shape for tissue penetration (Fig. 1A, B). The sensors have been electrically insulated by a

dielectric bilayer of Si_3N_4/Al_2O_3 (see Exp. Procedures). We refer to those probes as 'magnetrodes', for a magnetic equivalent of electrodes.

When a given input voltage is applied to the GMR sensors, their output voltage varies as a function of the in-plane component of the magnetic field. They exhibit a sensitivity of 10 to 25 $Volt_{out}/(Volt_{in}xTesla)$ (Fig. 1C). Their noise spectrum at a typical input voltage of 0.5 V leads to sensitivities of 7 nT/√Hz at 10 Hz, 2 nT/√Hz at 100 Hz and 370 pT/√Hz in the thermal noise regime above 1 kHz (Fig. 1D). We fabricated magnetrodes with sensing directions parallel to the tip (right magnetrode in Fig. 1B with sensing direction indicated by red arrow, i.e. 0° orientation) or orthogonal to the tip (left magnetrode in Fig. 1B with sensing direction indicated by green arrow, i.e. 90° orientation). When the magnetic sensing direction is parallel to the tip, magnetrodes are sensitive to electric currents flowing orthogonal to the tip. By contrast, when the magnetic sensing direction is orthogonal to the tip, magnetrodes are sensitive to currents running parallel to the tip (Fig. 1B).

We used two electronics schemes for the characterization of the sensors and for the *in-vivo* recordings; a DC mode and a modulation mode (AC mode) (Figure S1). The latter enables suppression of direct electric coupling between the probe and the neuropil and provides additional information concerning impedance changes in the medium (see Suppl.). In the AC mode, a small residual indirect coupling to electric fields, presumably due to a mixing in the silicon substrate, has been observed and quantified (see Suppl. And Figure S2).

Magnetic *in-vivo* recordings in the cat visual cortex

We performed *in-vivo* recordings in primary visual cortex of anesthetized cats (see Exp. Procedures). Figure 2 shows a schematic representation of the experimental setup. The magnetrode was inserted into the tissue to a depth of less than 1 mm from the cortical surface

126 using micromanipulators under microscope inspection. A tungsten electrode was placed within a
127 few hundred micron of the magnetrode to have a simultaneously recorded, independent electric
128 reference close to the magnetic sensor. To physiologically activate the recorded brain area, a
129 flash of light was shown directly into one eye of the cat. The duration of light stimulation was
130 either 100 ms or 500 ms, with a variable inter-stimulus interval of 0.9 to 1.5 s to avoid adaptation
131 or entrainment. The stimulus was presented 1000 times, and, after preprocessing, the output
132 signals (from the tungsten electrode and the magnetrode) were averaged with respect to stimulus
133 onset to calculate the event-related potential (ERP) for the electrode and the event-related field
134 (ERF) for the magnetrode (see Exp. Procedures).

135 Magnetic responses were recorded with magnetrodes sensitive to fields orthogonal to the tip, i.e.
136 fields parallel to the cortical surface (no signal has been observed with magnetrodes sensitive to
137 fields along the tip, see Suppl. and Fig. S3). Figure 3A and B show the results for the recordings
138 in the first animal (cat 1) with a stimulus duration of 100 ms. The GMR output in AC mode
139 shows a magnetic response starting 20 ms after stimulus onset, corresponding to the conduction
140 delay between the retina and the primary visual cortex. The ERF is characterized by a strong
141 negative component at 36 ms and a positive peak at 61 ms. The peak-to-peak amplitude was
142 2.5 nT. Figure 3C shows a magnification of the data with the ERF and ERP scaled and
143 superimposed to facilitate comparison. The onset of the electric signal is comparable to the
144 magnetic one, with a trough at slightly shorter latency and a peak at similar latency as the
145 magnetic signal.

146 Similar results were obtained in two separate recordings from another animal (Cat 2A and 2B).
147 Figures 3 D to F show the results for one recording site and a stimulation duration of 100 ms.
148 Figure 3 G to I present the data from another recording site later in the experiment with a

149 stimulation duration of 500 ms. With the longer stimulation, the on and off responses were
150 clearly separated, as evident in the magnetic and electric recordings. The signal amplitude of the
151 magnetic (and of the electric) recordings was larger than in cat 1, with a peak-to-peak amplitude
152 of around 10 to 12 nT. Similar to cat 1, the electric signal has a shorter latency than the magnetic
153 signal, but here the difference is only a few milliseconds. The overall shape of the ERF and ERP
154 were similar in all recordings performed.

155 **Signal quality evaluation**

156 To further characterize the magnetic responses, we calculated two metrics of signal quality. In a
157 first approach, we calculated the signal-to-noise ratio (SNR) of the ERFs and ERPs (see Exp.
158 Procedures and Suppl.) for increasingly large subsets of trials (Figure 4), to determine the
159 minimal trial number necessary for detection of a visually evoked response. As expected, the
160 SNR increased with increasing trial averaging (see also Figure S4). In comparison to the electric
161 recordings, the magnetic recordings showed a lower SNR, which grew more slowly with the
162 number of trials used to compute the average. Additionally, the recordings in cat 1 had a lower
163 SNR than those in cat 2, both, for the magnetic and electric recordings. We performed a
164 statistical test (random permutation test, $\alpha = 5\%$, n=1000 resamplings) to estimate the signal
165 detection threshold, that is to estimate the number of averages necessary to have a signal power
166 during stimulus presentation significantly larger than during the baseline period (dashed
167 horizontal lines in Figure 4A and B). In cat 1, 600 averages were necessary for the ERF to
168 become statistically significant. The two recordings in cat 2 allowed a statistically significant
169 ERF to be detected with 150 and 200 averages, respectively. For the electric recordings, all three
170 datasets show a significant ERP with 50 averages.

In a second approach, we quantified how the evoked responses (ERFs and ERPs), obtained from a certain number of trial averages, correlate with a template evoked response. This template was created from 50% of the trials, i.e. 500 trials. The other 50% were used to calculate evoked responses with an increasing number of averages. These test responses were then correlated to the template response using Pearson's correlation coefficient (see materials and methods for details).

Figure 4 C and D show the result of this analysis for the magnetic and electric recordings. As for the first method, cat 1 has an overall lower SNR, now reflected in smaller correlation values. Yet, even for the cat 1 dataset, the correlation became significant for ERFs averaging 75 trials (filled symbols show significant correlation values, bootstrap-test, see Materials and Methods). For the two datasets of cat 2, the correlation was already significant after averaging 50 (cat 2A) or merely 25 trials (cat 2B). As a further control for potential bias, we calculated the correlation between the stimulus-evoked template ERF and a surrogate ERF calculated from pre-stimulus data. These correlation values were close to zero and statistical tests against those bias estimates left the results unchanged.

DISCUSSION

In summary, we have shown that magnetrodes based on spin electronics can be used to record *in-vivo* magnetic signals originating from neuronal activity. This was possible, because GMR sensors combine a small size of a few tens of microns with sufficient magnetic field sensitivity. Local magnetic recordings can now open a new window onto neural activity. In addition, magnetic field recordings inside the tissue offer opportunities to better understand the commonly recorded extracranial MEG signal. There are also efforts to record neuronally generated

magnetic fields by means of magnetic resonance imaging (MRI) (Koerber 2013; Bandettini 2005), and magnetrodes could provide ground-truth measurements for this.

A potential concern stems from the currents required to measure the field-dependent resistance of the GMR sensor. Here, we used alternating currents (AC) because they allowed us to distinguish between on the one hand signals reflecting magnetic-field effects on the GMR and on the other hand voltages induced in the GMR by capacitive coupling to the tissue. Furthermore, by suppressing 50 Hz electric contamination, AC currents avoided preamplifier saturation and enhanced the signal to noise ratio. However, the AC currents might cause alternating magnetic fields that influence neuronal activity in the probe vicinity. Whether such influences exist at relevant magnitude will need to be investigated, yet it might be possible to minimize or entirely avoid AC currents in neuroscientific applications of the magnetrode. AC currents can be minimized through the use of more susceptible sensing elements, such as Tunnel Magneto-Resistance sensors, which would enable a higher or comparable sensitivity with a lower current amplitude (Polovy 2010). Also, for many applications, it will not be necessary to restrict the measured signals to currents that reflect magnetic fields, but any reflection of neuronal activity is of interest, whether mediated magnetically or through capacitive coupling. Those applications could use DC currents (potentially combined with magnetic shielding similar to current MEG recordings).

We would like to highlight the potential utility of GMR-based sensing of neuronal activity for recordings from un-tethered implanted devices. Implanted recording probes play an important role in many neurotechnological scenarios. Untethered probes are particularly intriguing, as they avoid connection wires and corresponding limitations (Seo 2016). Yet, for untethered probes to be maximally useful, they need to be tiny, and this results in a fundamental problem for electrical

recordings. Electrical recordings require two electrochemical interfaces with sufficient distance, such that the electrical potential difference does not become vanishingly small. The necessary distance restricts the size to which untethered devices based on electric recordings can be reduced. Magnetic field recordings do not suffer from this problem, because they require merely a singular GMR. Thus, magnetrode-based untethered recordings, while challenging, might provide a unique combination of recording and transmitting modalities for future neurotechnology.

We revealed visually evoked magnetic fields by averaging over multiple stimulus repetitions. This was possible, because the underlying postsynaptic potentials (PSPs) are long-lasting compared to their temporal jitter across trials. Thereby, PSPs temporally superimpose in the cross-trial average. This holds not only for PSPs of one postsynaptic neuron, but for PSPs of many neurons in the vicinity of the magnetrode. Thus, the ERF became detectable due to effective summation of the PSP-related magnetic fields across neurons and across trials. In one recording (cat 2B), the ERF after averaging merely 25 trials was already significantly correlated to the ERF after averaging an independent set of 500 trials (Figure 4C). This suggests that magnetic recordings might be able to detect not only ERFs but also action potentials (APs). In electric recordings, isolated single neurons typically generate AP waveforms of the same size or larger than the ERPs generated by the summation of many neurons. This is likely due to the fact that each AP reflects massive transmembrane current flows that are sufficient to move the intracellular potential across the cell body from -60 mV relative to the extracellular space to +30 mV. Whether these current flows generate detectable magnetic fields will crucially depend on their spatial symmetry and their temporal simultaneity. If all involved currents flew simultaneously and with spherical symmetry, they would generate no detectable magnetic field.

However, it is known that APs emerge in the axon hillock and retrogradely invade the cell body and sometimes the dendrites (Mc Cormick 2007, Stuart 1997). Nevertheless, magnetic recordings of APs will be challenging, because averaging across trials will typically not be an option. If such recordings succeed, they would hold great promise. Single microelectrodes typically record APs from merely a handful of neurons, because insulating cell membranes isolate them from the hundreds of neurons in their immediate vicinity (Buzsàki 2004). Magnetic fields from APs should travel from neurons to the magnetrode without attenuation. This might enable the recording of tens or even hundreds of neurons from the vicinity of the magnetrode. The separation of APs originating from different neurons will benefit from the vectorial nature of magnetic sources and the corresponding vectorial sensitivity of the sensors. Sensors specific for the three spatial dimensions could be combined on a single magnetrode to estimate the 3D position of each neuronal source relative to the magnetrode.

EXPERIMENTAL PROCEDURES

In-vivo recording procedures and data analysis

The animal experiments were approved by the responsible government office (Regierungspräsidium Darmstadt) in accordance with the German law for the protection of animals. Two adult cats (1 male, 1 female) were used for visual neuroscience experiments, after which magnetrodes were tested. Anesthesia was initiated intramuscularly with 10 mg/kg ketamine hydrochloride (Ketavet, Zoetis, Germany) and 0.05 mg/kg dexmedetomidine (Dexdormitor, Orion Pharma, Germany) supplemented with 0.04 mg/kg atropinesulfat (Atropin, B.Braun, Germany). Anesthesia was maintained after tracheotomy by artificial ventilation with a mixture of N_2O/O_2 (70/30%) with 0.8% isoflurane. Analgesia was maintained by intravenous infusion of sufentanil (2 µg/kg/h, Sufentanil-Hameln, Germany) together with electrolytes (3 ml/kg/h, Sterofundin, B.Braun, Germany) and glucose (24 mg/kg/h, bela-pharm, Germany). After all surgical procedures had been terminated, the animals were paralyzed by intravenous infusion of

263 vecuronium bromide (0.25 mg/kg/h, Vecuronium-Inresa, Germany). Depth of anesthesia was controlled
264 by continuously monitoring the electrocardiogram and CO_2 level. Dexamethasone (Voren, Boehringer
265 Ingelheim, Switzerland) was administered every 48h and if needed. A craniotomy was performed around
266 the central part of the primary visual cortex area 17 (homologue to V1 in primates, Horsley–Clarke
267 coordinates AP -2 to -10, ML 0 to +6) and area 21a (homologue to V4 in primates, Horsley–Clarke
268 coordinates AP 0 to -8, ML +8 to +15), a higher visual area of the ventral pathway. The dura mater was
269 removed in a small window to allow easy insertion of the recording probes.

270 Electrical recordings were performed with tungsten electrodes (1 MΩ impedance, FHC, USA). The
271 electrode and the magnetrode were held by separate micromanipulators (David Kopf Instruments, USA)
272 allowing for a precise positioning and careful insertion into the cortex under microscope inspection. The
273 magnetrode was inserted first, about 1 mm below the cortical surface, and angled such that the probe
274 penetrated the cortex as perpendicularly as possible. Subsequently, the tungsten electrode was inserted in
275 close vicinity to the magnetrode. Given the cortical thickness of the cat, the sensors were expected to be
276 located near cortical layer 4, the input layer. Signals from the magnetrode in AC or DC mode, as well as
277 from the electrode were recorded with a standard acquisition system (Tucker Davis Technologies, USA).
278 To this end, the signals were buffered by a unity gain headstage, low-pass filtered at 100 Hz and digitized
279 at 1017 Hz.

280 For visual stimulation, a brief (100 or 500 ms) flash of light was applied directly to the contralateral eye
281 of the cat. This light flash (473 nm wavelength) was applied through a glass fiber (2 mm diameter) ending
282 close to the cornea and driven by an LED (Omicron-laserage, Germany) with an output intensity of about
283 2-10 mW at the end of the fiber. Atropine (Atropine-POS 1%, Urspharm, Germany) was topically applied
284 to the eye in order to dilate the pupil. The glass fiber and the animal's forehead were shielded with
285 aluminum foil, to ensure that no light reached the magnetrode. This is important, because the
286 magnetrode's silicon substrate could be directly influenced by the light flash, i.e. by the photoelectric
287 effect. However, the detected magnetic signals have a latency of 20-40 ms, which corresponds to the

conduction delay from the retina to the cortex, ruling out a direct effect of the light flash on the magnetrode. To generate the light flash, the LED was controlled by the same unit that also controls the data recordings (RZ2, Tucker Davis Technologies, USA). Several recording sessions were performed, each comprising 1000 to 2000 light flash repetitions. The light flash had a duration of 100 or 500 ms depending on the session. The inter-stimulus interval was 0.9 s plus a random time between 0 and 0.6 s to prevent adaptation or entrainment of the cortex to the repeated visual stimulus.

Offline data processing and analysis was done by custom written software and the FieldTrip toolbox (Oostenveld et al., 2011) coded in Matlab (The Mathworks, USA). First, line noise artifacts were removed by a second-order bandstop Butterworth filter at the power line frequency (50Hz +/- 1Hz, including its harmonics up to 250Hz). Subsequently, data were averaged across trials, aligned to the light flash onset. This extracts the stimulus-locked (i.e. evoked) brain activity, and averages out all other internal or external fluctuations unrelated to the stimulus.

Signal quality estimation

To assess the quality of the magnetic ERF recordings with respect to increasing the number of trials used to compute the averages, we applied two measures of signal quality. In the first approach, we quantified the signal-to-noise ratio (SNR) of the stimulus evoked magnetic recording defined as:

$$SNR(dB) = 10 \times log_{10}\left(\frac{P_S}{P_N}\right) \qquad (1)$$

Where P_s is the power of the signal and P_N the power of the noise. The power was quantified as the mean squared response to the stimulus in a specific window (after removing a second order polynomial to avoid high power values due to slow drifts). Because the visual cortex usually responds to the onset and offset of a stimulus (see Figure 3), we choose a window of 150ms after stimulus onset and offset for signal quantification. For the 100ms long stimulus, however, onset and offset responses overlap in time, and the resulting window was chosen from 0 to 250ms (i.e. 150ms after the offset). For the 500ms long stimulus, the total window length was 300ms (from 0 to 150ms and from 500 to 650ms, See figure S7). For both

312 stimuli, an equally long window was chosen before stimulus onset to quantify the noise. We note here,
313 that this definition of stimulus and noise is different from previous studies, which assume a model of
314 additive (Gaussian) noise on top of a constant stimulus (Turetsky et al., 1988). SNR is then calculated
315 from an estimation of the signal and noise components of the recorded stimulus evoked signal. However,
316 we think that using the ongoing brain activity (baseline) as a measure of 'noise' is more intuitive because
317 the SNR then quantifies the amount of stimulus locked activity, without making assumptions about the
318 nature of different sources of noise. For simplicity, we keep the nomenclature of 'signal' and 'noise' for
319 'stimulus evoked' and 'baseline' activity.

320 We were interested in how the quality of the average signal (ERF/ERP) improves with an increasing
321 number of trials, e.g. stimulus presentations (Figure 4 and S7). Therefore, we calculated the SNR
322 (equation 1) for a random subset of trials, increasing the sample size successively. For each step (50, 100,
323 150, … trials), we repeated the random draw ten times and averaged the ten SNRs to get a more stable
324 estimate. We also tested the significance of the SNR value using a permutation test with multiple
325 comparison correction (Maris and Oostenveld, 2007). First, we obtained the permutation distribution
326 under the null-hypothesis of no difference between signal and noise. We randomly labeled each trial as
327 occurring before stimulus onset (i.e. noise) or after stimulus onset (i.e. signal), irrespective of its true
328 identity. Then, the SNR, after obtaining the noise and signal power from these randomized epochs, was
329 calculated the same way as for the non-randomized data (10 times from 10 different subsets). However,
330 instead of averaging the SNR for the 10 different draws for a given subset, the 10 SNR values entered the
331 permutation distribution. This is because otherwise the width of the permutation distribution will
332 approach zero for an increasing number of random draws. The complete procedure was repeated 1000
333 times to obtain the permutation distribution. Then, the smallest and largest SNR across the sample size
334 steps was stored for each of the 1000 permutations. From this distribution of largest and smallest SNRs,
335 the 2.5^{th} and 97.5^{th} percentile represents the significance threshold corresponding to a two sided test with

an alpha level of 5% and a correction for multiple comparisons across sample size steps (Nichols and Holmes, 2002).

In a second approach, we asked how similar the evoked responses of a small subset of trials is to the corresponding evoked response of a large subset of trials. To this end, we first randomly partitioned the trials in two groups. The data in the first group was averaged across all trials (n=500), and the data around stimulus onset and offset (Same window as described above) served as the template for the ERF/ERP. The second group was partitioned in smaller subsets with an increasing number of trials (25, 50, 75, … 500) and for each subset the data was averaged to obtain the test-sample. Then, for each subset, the test-sample was correlated (Pearson's correlation coefficient) with the template. This procedure was repeated 1000 times, each time drawing randomly the trails for the test-sample and the template. The resulting 1000 correlation coefficients at each step were then averaged. Because these 1000 correlation coefficients are essentially a bootstrap distribution, we estimated the 95% confidence interval directly by taking the 2.5^{th} and 97.5^{th} percentiles of this distribution to check for significant correlations. To assess the sensitivity and a potential bias of this measure, we tested the null hypothesis of no relationship between template and sample, by taking the sample from the baseline period.

SUPPLEMENTAL INFORMATION

Supplemental Information includes Supplemental Experimental Procedures and seven Figures.

AUTHOR CONTRIBUTIONS

Conceptualization, M.P.L., C.F. and P.F.; Methodology: L.C., J.T.R., J.P.A., J.V. and V.T.; Investigation: T.W., C.M.L., J.N., L.C., J.P.A., J.V., S.C., P.P.F., C.F. and M.P.L.; Analysis: T.W., V.T. and C.M.L.; Writing – Original draft: M.P.L., T.W. and P.F. Funding Acquisition: M.P.L. , P.P.F. and P.F.

ACKNOWLEDGMENTS

This work has been funded through the EU Project Magnetrodes (FP7-ICT-2011 project 600730) and through the Magsondes project by RTRA-Triangle de La Physique. This work was partly supported by

the french RENATECH network. INESC-MN acknowledges FCT funding through project EXCL/CTM-NAN/0441/2012 and the IN Associated Laboratory. ESI acknowledges funding through the DFG (FOR 1847, SPP 1665, FR2557/5-1-CORNET), the EU (HEALTH F2 2008 200728, HBP), the NIH (HCP WU-Minn Consortium, NIH grant 1U54MH091657), and the LOEWE program (NeFF).

REFERENCES

Amaral, J., Sebastião, A.M., Cardoso, S., and Freitas, P.P. (2011). Towards a system to measure action potential on mice brain slice with local magneto resistive probes, J. Appl. Phys. *109*, 07B308.

Baibich, M.N., Broto, J.M., Fert, A., Nguyen Van Dau, F., Petroff, F., Etienne, P., Creuzet, G., Friederich, A., Chazelas, J. (1988). Giant magnetoresistance of (001)Fe/(001)Cr magnetic superlattices. Phys. Rev. Lett. *21,* 2472.

Bandettini P.A., Petridou N., Bodurka J. 2005. Direct detection of neuronal activity with MRI: fantasy, possibility, or reality? Appl Magn Reson *29*:65–88.

Barnes, B., and Greenebaum, B. (2006). Biological and Medical Aspects of Electromagnetic Fields (CRC Press Taylor & Francis Group).

Barry, J.F., Turner, M.J., Schloss, J.M., Glenn, D.R., Song, Y., Lukin, M.D., Park, H., Walsworth, R.L. (2016). Optical magnetic detection of single-neuron action potentials using quantum defects in diamond. arXiv:1602.01056 .

Buzsáki, G. (2004). Large-scale recording of neuronal ensembles. Nat. Neurosci. *7*, 446–451.

Buzsáki, G., Anastassiou, C.A., Koch, C. (2012). The origin of extracellular fields and currents--EEG, ECoG, LFP and spikes. Nature reviews. Neuroscience *13*, 407.

Buzsáki, G., and Draguhn, A. (2004). Neuronal oscillations in cortical networks. Science *304*, 1926.

383 Cohen, D. (1968). Magnetoencephalography: Evidence of Magnetic Fields Produced by Alpha-
384 Rhythm Currents, Science *161,* 784-786.
385 Cohen, D. (1972). Magnetoencephalography: Detection of the Brain's Electrical Activity with a
386 Superconducting Magnetometer, Science *175,* 664-666.
387 Dieny, B., Speriosu, V.S., Parkin, S.S.P., Gurney, B.A., Wilhoit, D.R., and Mauri, D. (1991).
388 Giant magnetoresistive in soft ferromagnetic multilayers. Phys. Rev. B**.** *43*, 1297–1300.
389 Kandel, E. R., Schwartz, J.H., and Jessel, T.M. (2000). Principles of Neural Science (MGraw-
390 Hill, ed. 4).
391 Koerber, R., Nieminen, J. O., Hoefner, N., Jazbinšek, V., Scheer, H. J., Kim, K., Burghoff M.
392 (2013) An advanced phantom study assessing the feasibility of neuronal current imaging by
393 ultra-low-field NMR , Journal of Magnetic Resonance *237* 182-190.
394 Lewis, C.M., Bosman, C.A., Fries, P. (2015). Recording of brain activity across spatial scales,
395 Current Opinion in Neurobiology *32*, 68-77.
396 Magnelind, P. (2006). High-Tc SQUIDs for magnetophysiology - development of a
397 magnetometer system and measurements of evoked fields from hippocampal neurons in-vitro.
398 PhD thesis, Chalmers University of Technology.
399 Maris, E., Oostenveld, R. (2007). Nonparametric statistical testing of EEG- and MEG-data.
400 Journal of neuroscience methods. *164*, 177.
401 Maynard, E.M., Nordhausen, C.T., Normann, R.A. (1997). The Utah Intracortical Electrode
402 Array: A recording structure for potential brain-computer interfaces. Electroencephalogr. Clin.
403 Neurophysiol. *102*, 228-239.
404 McCormick D.A. , Shu Y., Yu Y. (2007). Hodgkin and Huxley model--still standing? Nature
405 *4;445* (7123):E1-2; discussion E2-3.

406 Nichols, T.E., and Holmes, A.P. (2002). Nonparametric permutation tests for functional
407 neuroimaging: a primer with examples. Hum. Brain Mapp. *15*, 1–25.

408 Oostenveld, R., Fries, P., Maris, E., Schoffelen, J.M. (2011). FieldTrip: Open source software for
409 advanced analysis of MEG, EEG, and invasive electrophysiological data. Computational
410 intelligence and neuroscience. *2011*, 156869.

411 Polovy, H., Guerrero, R., Scola, J., Pannetier-Lecoeur, M., Fermon, C., Feng, G., Fahy, K.,
412 Cardoso, S., Almeida, J., Freitas, P.P. (2010) Noise of MgO-based magnetic tunnel junctions,
413 Journal of Magnetism and Magnetic Materials, *322*, p1624–1627.

414 Roth, B.J., and Wikswo, J.P. (1985). The magnetic field of a single axon. a comparison of theory
415 and experiment. Biophys. J. *48*, 93–109.

416 Sander, T. H., Preusser, J., Mhaskar, R., Kitching, J., Trahms, L., & Knappe, S. (2012).
417 Magnetoencephalography with a chip-scale atomic magnetometer. Biomedical Optics Express,
418 *3*(5), 981–990.

419 Seo, D., Neely, R. M., Shen, K., Singhal, U., Alon, E., Rabaey, J. M., Carmena, J. M., Maharbiz,
420 M. M. (2016). Wireless Recording in the Peripheral Nervous System with Ultrasonic Neural
421 Dust. Neuron, 3;*91*(3):529-39.

422 Stuart G., Spruston N., Sakmann B., Häusser M. (1997). Action potential initiation and
423 backpropagation in neurons of the mammalian CNS. Trends Neurosci. *20(3)*:125-31.

424 Turetsky, B.I., Raz, J., Fein, G. (1988). Noise and signal power and their effects on evoked
425 potential estimation. Electroencephalography and clinical neurophysiology. *71*, 310.

426

FIGURE LEGENDS

Figure 1. Magnetrode description and magnetic characteristics. **(A)** Scanning Electron Microscopy picture of a magnetrode containing 2 GMR elements, each with a meandering configuration. The elements are deposited on a 200 µm thick silicon substrate that is 150 µm wide before narrowing at an 18° angle towards the tip. The sensitive direction is in the plane of the elements and orthogonal to the long axis of the tip (90°). A platinum electrode (blue square) has additionally been deposited, but no recordings were achieved with it. Scale bar 100 µm. **(B)** Schematics of two magnetrodes with different sensing directions. Left side: GMR elements sensitive to magnetic field components orthogonal to the tip direction (green arrow). Right side: GMR elements sensitive to magnetic field components parallel to the tip direction (red arrow). A current flowing through a neuron extended along the tip of the magnetrodes exhibits field components along B_x and B_y, thus measurable on the magnetrode shown on the left side**. (C)** Inset: Simplified representation of GMR stack. The reference layer (or pinned layer), whose magnetization is set perpendicularly to the long axis of the meandering circuit path (violet arrow), comprises an antiferromagnet-PtMn (violet) magnetically coupled to an artificial antiferromagnet, composed of two CoFe layers (dark blue) separated by a thin Ru layer (light pink). The free layer is made up of a CoFe layer (dark blue) coupled to a NiFe layer (light blue) presenting a very low coercive field that enables an easy rotation of the bilayer magnetization (light blue arrow) when an in-plane field is applied. Pinned and free layer are separated by a thin copper layer (orange) that provides a magnetic decoupling of two layers. The pinned layer direction defines the sensitive direction of the GMR element. The line graph shows the output voltage of the GMR meander as a function of a magnetic field applied along the pinning direction. When the field is applied in the same direction, spin transport is facilitated and resistance is lowest, whereas when the field is applied in opposite direction, electrons experience a higher scattering and resistance is largest. The sensor is used for very weak magnetic fields around zero, that lead to outputs within the steep linear part of the curve. In the linear part, the slope is 1.8%/mT. **(D)** Equivalent-field noise spectral density S_B from 1 Hz to 10 kHz of the corresponding probe for 500 mV

and 1 V peak-to-peak AC voltage of the GMR element. To obtain S_B, the output voltage is converted in field-equivalent by applying a calibrated magnetic signal at 30 Hz.

Figure 2. Schematic representation of the experiment. Recordings are performed in primary visual cortex of the anesthetized cat. To activate these areas, a visual stimulus is applied directly to the contralateral eye using blue laser light. The magnetrode, containing one or two GMR sensors, is positioned within the visual cortex. A tungsten electrode is placed in the vicinity of the magnetrode as a control. The output signals from the GMR sensor and from the electrode are amplified, filtered and sent through an acquisition channel. An example of an ERP from the electrode (top) and the simultaneously recorded ERF (bottom) from the magnetrode is shown to the right. An illustration of the expected configuration of the probe's location within the neuropil is presented in the left side inset.

Figure 3. *In-vivo* neuronal signals recorded simultaneously on the tungsten electrode and on the magnetrode.

Data from three recording sessions (in two cats) are presented (rows). The mean (+/- SEM) magnetic signal recorded from the magnetrode is shown in red, and the simultaneous recorded electric signals from the tungsten electrode in green. Stimulus onset and offset is indicated by vertical dashed lines. Panels C, F and I show magnifications of the ERFs and ERPs around stimulus onset, with the vertical axes scaled to facilitate comparison between the ERP and ERF shape.

Figure 4. Recording quality.

(A, B) Signal-to-noise ratio (SNR) quantification for the magnetic (A) and electric (B) recordings. Data are color coded for the three sessions presented in figure 3. An SNR above the significance threshold (horizontal dashed line, permutation test $p<0.05$) is given by filled symbols. Note the different scaling of the y-axis for the magnetic and electric recordings.

(C, D) Pearson correlation of evoked responses with a given number (x-axis) of averages to a template obtained by averaging 50% of the trials. Note that the correlation values for ERPs of cat2A and cat2B

476 (panel D) are very similar and appear to largely overlap. Filled circles indicate significant correlation
477 values.

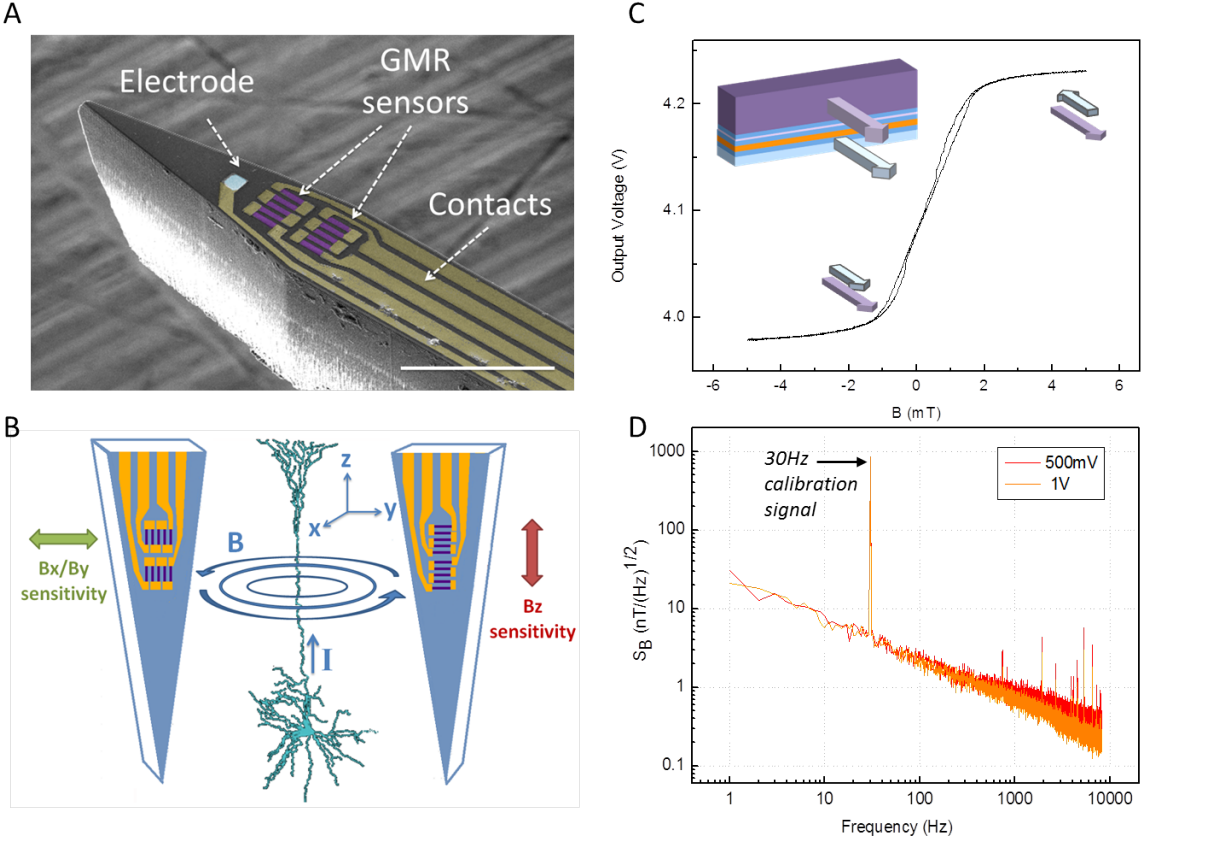
A
Electrode
GMR sensors
Contacts
B
Bx/By sensitivity
B
z
y
x
I
Bz sensitivity
C
Output Voltage (V)
4.2
4.1
4.0
-6
-4
-2
0
2
4
6
B (mT)
D
30Hz calibration signal
500mV
1V
S_B (nT/(Hz)$^{1/2}$)
1000
100
10
1
0.1
1
10
100
1000
10000
Frequency (Hz)

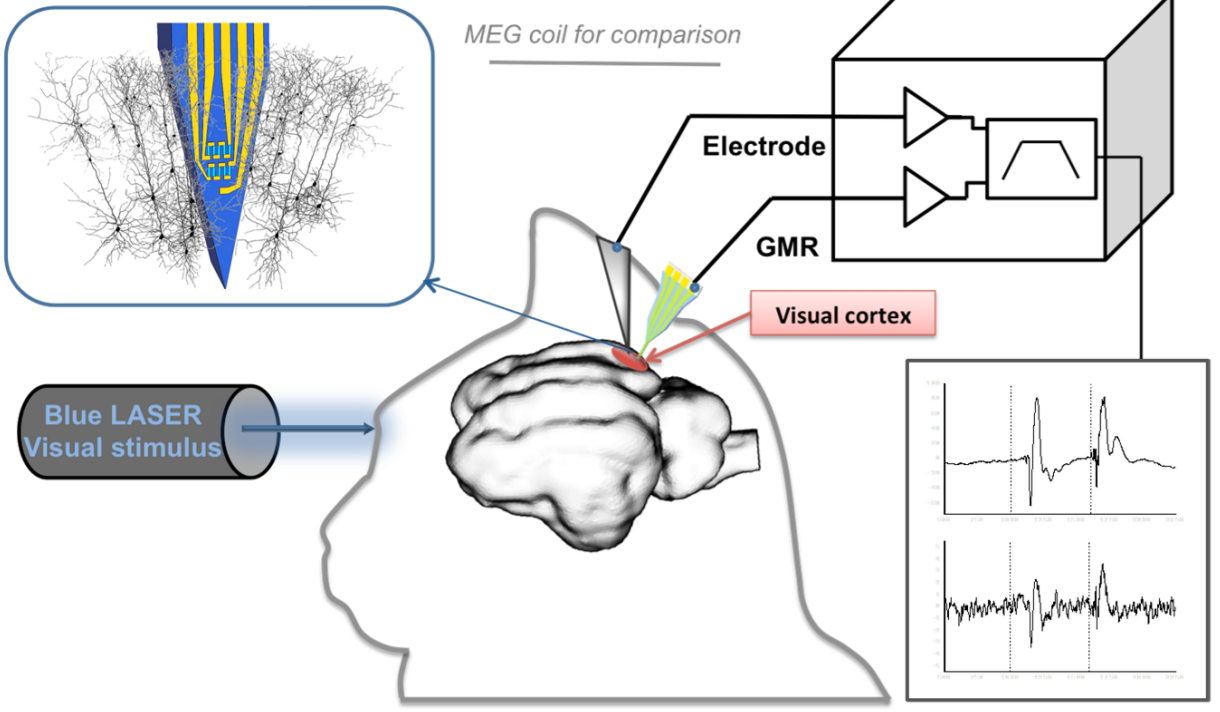
MEG coil for comparison
Electrode
GMR
Visual cortex
Blue LASER
Visual stimulus

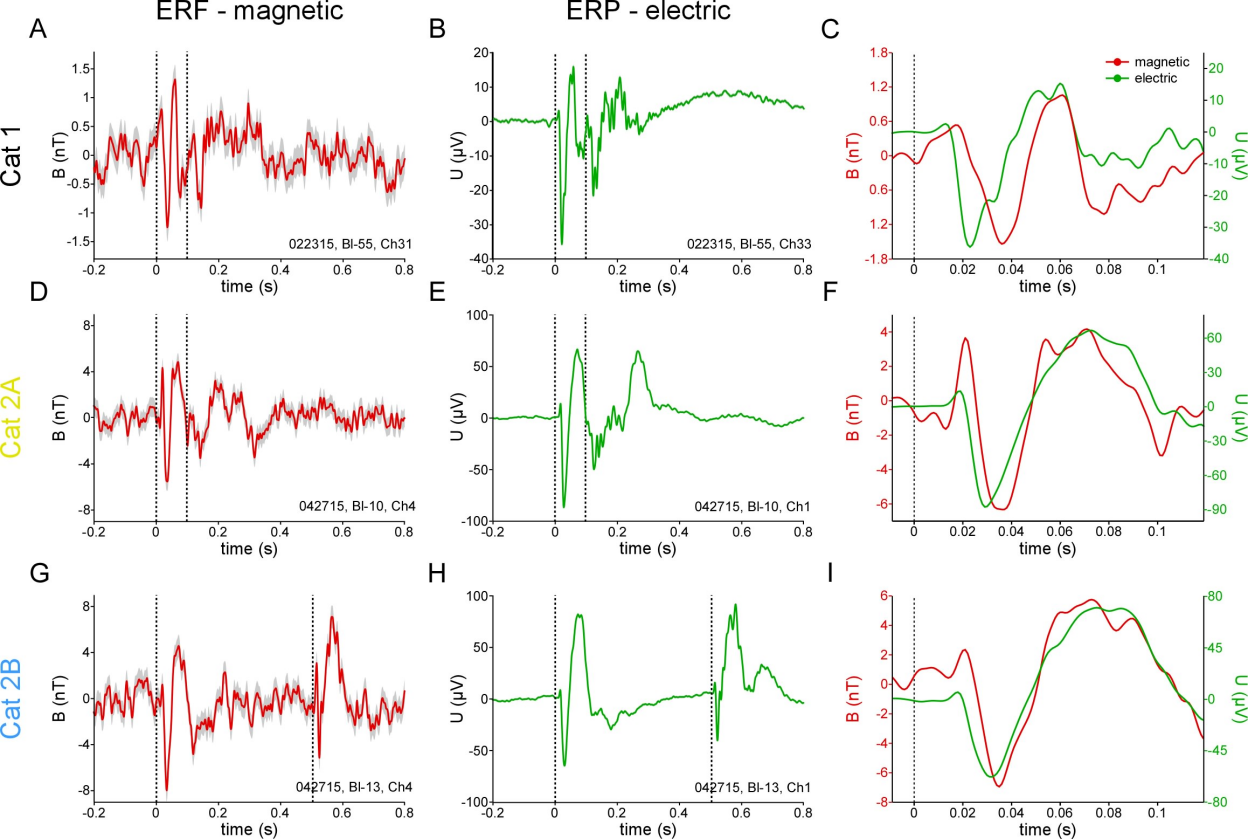
ERF - magnetic
ERP - electric
A
B
C
Cat 1
B (nT)
U (μV)
time (s)
022315, Bl-55, Ch31
022315, Bl-55, Ch33
magnetic
electric
D
E
F
Cat 2A
042715, Bl-10, Ch4
042715, Bl-10, Ch1
G
H
I
Cat 2B
042715, Bl-13, Ch4
042715, Bl-13, Ch1

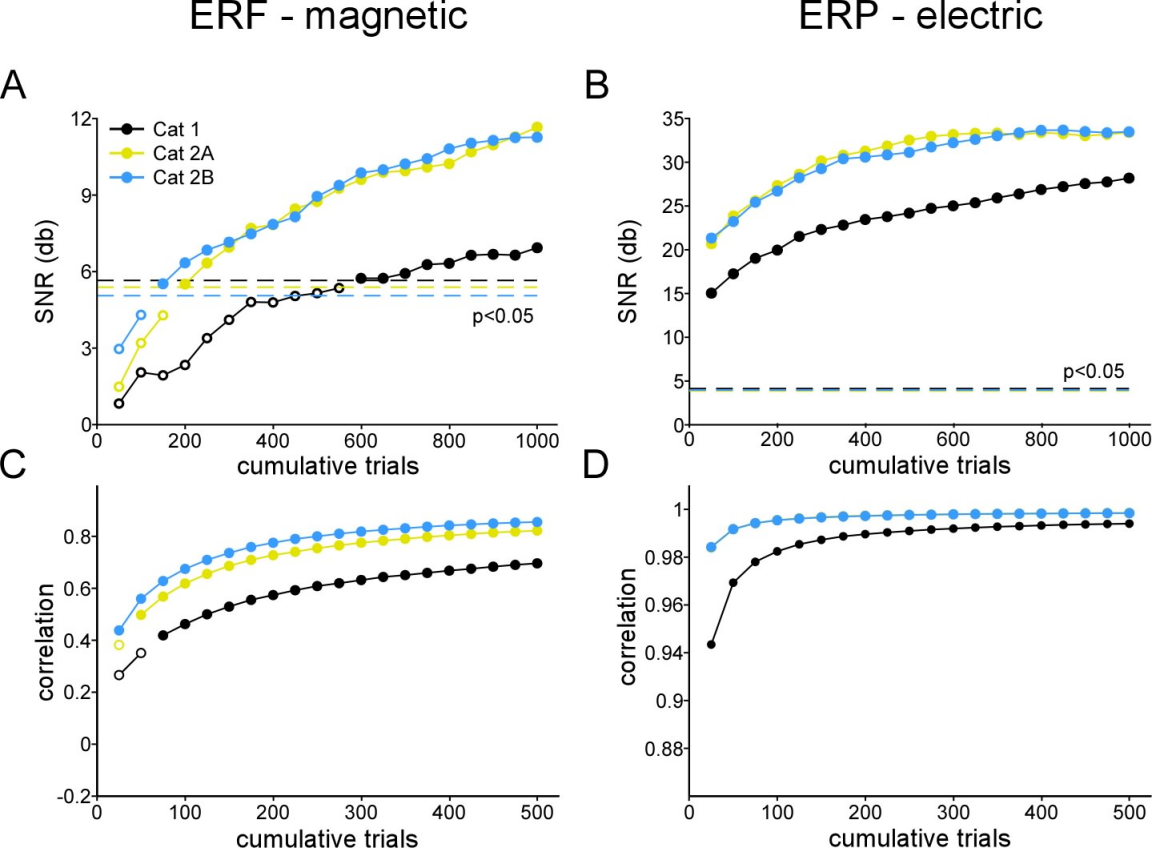
ERF - magnetic
ERP - electric
A
B
C
D
Cat 1
Cat 2A
Cat 2B
SNR (db)
p<0.05
cumulative trials
correlation